NiFe Plated Biaxial MEMS Scanner for 2-D Imaging

Arda D. Yalcinkaya, Hakan Urey, and Sven Holmstrom

***Abstract*—A two-axis microelectromechanical systems micromirror actuator is developed for retinal scanning display and imaging applications. The device operation makes use of magnetostatic torque produced by the combination of a flux generating custom-made high-frequency electrocoil and the NiFe layer deposited on the movable part. Modeling of the actuation in the magnetic domain, as well as the experimental characterization of the mechanical part is described. The device is capable of full optical scan angles of 88° (at 100-mA root-mean-square coil current) and 1.8° for slow and fast-scan directions, respectively. In combination with a mirror size of 1.5 mm, resulting $\theta_{\rm opt} \cdot D$ products are 132°· mm and 2.7°· mm for slow and fast axis, respectively. Atmospheric operation of the device is enabled due to high mechanical quality factors of the order of 3000.**

***Index Terms*—Displays, electromagnetic actuator, microelectromechanical systems (MEMS), microsystems, microtechnology.**

I. Introduction

AMONG the ways of constructing displays, scanned light beam displays constitute a major place utilizing a mirror producing angular motion to deflect a modulated light beam on an image plane. The core of such a display system is the microscanner, a device that can produce two-dimensional (2-D) motion in the orthogonal axis, with significant scan angles. Scanners are used in applications such as automotive head-up displays and headworn displays [1]–[3] and in barcode scanning [5], [6], endoscopy [7], optical switching [8], and other general applications [9]. There are a number of challenges in designing microelectromechanical systems (MEMS) scanners for display systems. For instance, since the scanner represents the system's limiting aperture, a sufficient size for the scanning mirror is required. In addition to that, the mirror flatness must be smaller than one-tenth of the wavelength of the laser beam in order not to distort the beam's wave front. The fast-scan frequency has to be high enough to handle the many millions of pixels per second. Two-axis scan over significant angles has to be performed in order to paint a wide-angle 2-D image [1], [5], [8], [10], [11]. There have been some attempts to realize permalloy-based magnetostatic one-dimensional (1-D) optical scanners [4] and actuators [13], but to the authors' knowledge, there is no 2-D MEMS scanner based on a magnetostatic scanner published in the literature. Using the presented new actuation method, the first 2-D magnetostatic MEMS scanner design has been implemented satisfying the requirements of a variety of display and imaging applications.

Manuscript received November 17, 2006; revised December 21, 2006. This work was supported by TUBITAK under Project MISAG-280-2004.

A. D. Yalcinkaya is with the Electrical and Electronics Engineering Department, College of Engineering, Bogazici University, Bebek TR-34342, Istanbul, Turkey (e-mail: arda.yalcinkaya@boun.edu.tr).

H. Urey and S. Holmstrom are with the Electrical and Electronics Engineering Department, College of Engineering, Koc University, Sariyer TR-34450, Istanbul, Turkey (e-mail: hurey@ku.edu.tr; sholmstrom@ku.edu.tr).

Color versions of one or more of the figures in this letter are available online at http://ieeexplore.ieee.org.

Digital Object Identifier 10.1109/LPT.2007.891592

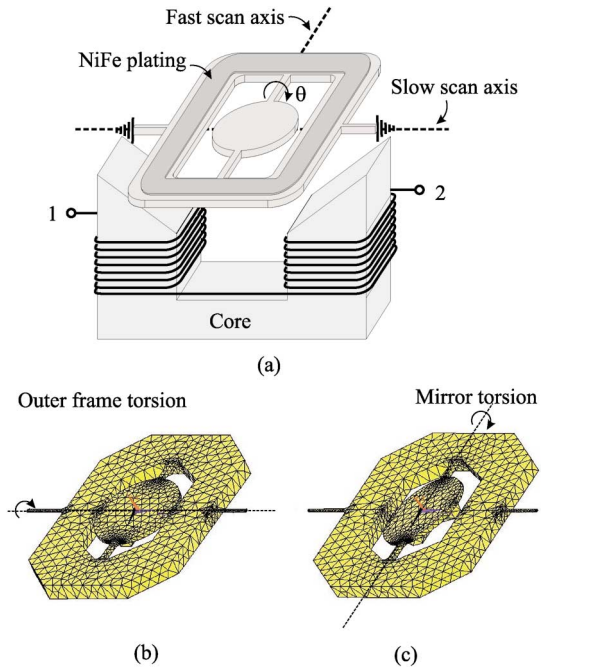

Fig. 1. (a) Schematic of the microscanner operation setup. The electrocoil driven at the ports labeled as 1 and 2 creates the magnetic flux. (b) FEM simulation showing the torsion mode of the outer frame (slow-scan operation). (c) FEM simulation showing the coupling of the rocking mode to the torsion mode of the mirror.

II. Magnetostatic Actuator Operation

Schematic representation of the device along with the actuation setup is given in Fig. 1. The device is composed of a circular mirror, gimbal mounted to an outer frame. The outer frame is anchored to a fixed substrate through a set of springs. A thin soft-magnetic NiFe layer is selectively deposited on the outer frame by means of electroforming. The actuation is driven by a custom-made flux generator that consists of coil turns wound on high permeability core. When an alternating current is passed between Ports 1 and 2, a frequency-dependent magnetic field (and flux) is created in the direction normal to the scanner plane. Along with a permanent magnet aligned with the NiFe layer, the external magnetic field induces bidirectional force components on the magnetic layer. A very similar mechanical structure is used in [1] where the actuation is driven by the Lorentz force. In comparison with the device in [1], the present device offers the following advantages: 1) having a potentially simpler fabrication due to a lower number of lithographical steps for plating base definition ([1] requires at least two masks for coil fabrication, whereas the present device uses one mask layer for plating base definition for electroforming); 2) requiring no wire bonds, since the actuation is driven with an off-chip coil. Operation of

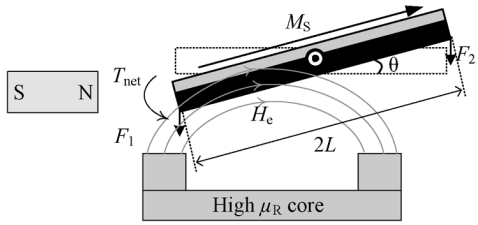

Fig. 2. Simplified schematic of the scanner operation principle. The scanner is placed with a slight offset in reference to the electrocoil in order to create a net moment.

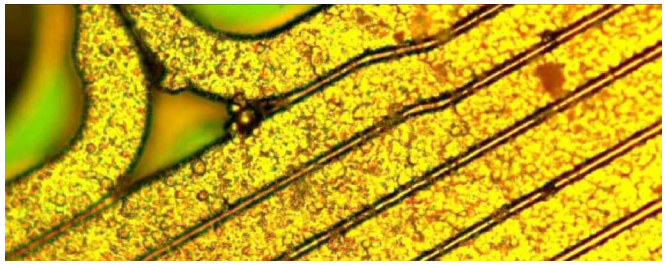

Fig. 3. Optical microscope photo of the plated magnetic layer on the outer frame. NiFe is deposited on existing Au coil windings for convenience (coil structure is not needed).

the device is simulated using a finite-element method (FEM) structural mechanics simulation tool. The FEM result shown in Fig. 1(b) and (c) shows the rotation about the slow-scan axis (torsion) and the rotation about the fast-scan axis (rocking) at the designed mode frequencies. Utilization of the permanent magnet creates a predefined magnetization. Fig. 2 gives a simplified schematic of the scanner-electrocoil interaction, where the scanner is placed with some amount of offset with respect to the center of the electrocoil. The magnetic forces lumped to the edges of the microstructure are marked with F_1 and F_2, respectively. The magnitude of these forces can be expressed as [13]

$$F_i = M_s \cdot W \cdot t \cdot H_{ei} \tag{1}$$

where $F_i (i = 1, 2)$ is the magnetostatic force, M_s is the saturation magnetization, H_{ei} is the magnetic field at the respective point, W and t are the width and the thickness of the NiFe layer. The magnetization vector is assumed to stay in the plane of the NiFe deposit plane, mainly due to shape anisotropy phenomenon. The reason for shape anisotropy in this structure is the ratio between the length (or the width) and the thickness of the NiFe layer $(2L/t \gg 50)$ [14]. In the presence of a permanent magnet next to the NiFe plate, magnetization direction remains the same and the force direction is controlled by the current direction in the electrocoil; thus, the force could be directional. Since the magnetic material is saturated by the existence of a net radial field of about 5 mT, the dc field induced by the permanent magnet has to be 5 mT higher than the ac radial field created by the coil. When there is no permanent magnet, the force is always attractive since there is no preferred direction for the magnetization within the plane. A net moment is induced on the scanner related to the force components and the moment arm with the length of L, that lies between the connection point and the position of the lumped force. This total net moment is

$$T_{\text{net}} = (F_1 - F_2) \cdot L \cos(\theta) \tag{2}$$

where θ is the rotation angle of the outer frame referenced to the rest position. In the case where the scanner's and the electrocoil's centers are aligned and $\theta = 0$, there will be no net torque because both of the forces at the edge of the device have equal size and the same direction (i.e., both attractive). A slight offset is sufficient to tip the balance and to obtain a sufficient net torque. When the frequency of the magnetic force enters into the passband of the scanner's mechanical resonance, the device rotation is amplified by the quality (Q) factor of the torsion mode. The fast-scan mode of the scanner is driven as shown in Fig. 1(a) and the slow scan is driven by positioning the electrocoil perpendicular to its initial place. In the fast-scan mode, a small displacement of the outer frame is coupled to the circular scanning mirror. This coupled motion is multiplied with the mechanical Q-factor of the mirror to produce the fast-scan angle [1], [2].

III. Experimental Results

The device is fabricated by using silicon bulk micromachining in combination with post metal plating processes. The electrodeposited magnetic layer is $Ni_{80}Fe_{20}$ deposited on the existing Au coil windings (instead of the coil wires, a more suitable plating area can be defined by changing the preprocessing of the Si structure) with an average thickness of 8 μm (see Fig. 3). The present scanner does not carry any electrical signals on the movable part which not only helps to maintain a fixed Q-factor (i.e., all the electrical interconnects that may result in fatigue problems and thus Q-factor changes are eliminated), but also removes problems associated with self heating, which can as well create fluctuations in Q-factor due to temperature-related stress gradients at the suspensions. Characterization of the scanner is performed by driving the electrocoil (coil resistance: 17 Ω) with a sinusoidal signal of varying frequency and detecting the resulting mirror displacement with a laser Doppler vibrometer at every frequency step. All the characterizations are performed in ambient air and no special precautions are taken to reduce film damping.

A. Slow-Scan Sinusoidal Drive (Resonance Behavior)

Mechanical resonance of the slow-scan motion (torsion mode of the outer frame) occurs at 367 Hz. Fig. 4(a) shows the total optical scan angle (TOSA) of the scanning mirror as a function of frequency. For Q-factor measurements, the electrocoil drive current is kept low (410 μA), yet 4° of optical scan angle is obtained consuming a root-mean-square power of 2.87 μW. When the drive power is increased to 170 mW, the optical scan angle goes up to $\theta = 88°$. Fig. 4(b) shows a 1-D scan image created by the present scanner at 60 Hz dissipating 27 mW. The scanline, which measures 3.4 cm, appears at 20 cm away from the device corresponding an optical scan angle of 9.6°. This experiment clearly states that the scanner is suitable for off-resonance operation.

B. Fast-Scan Sinusoidal Drive (Resonance Behavior)

Fast-scan resonance (torsion mode of the mirror) occurs at 22230 Hz. Fig. 4(c) depicts the TOSA of the mirror as a function of frequency. The peak optical angle is 1.8° at a drive current of 3 mA. The fast axis resolution that can be achieved with the present performance is limited to 50 pixels, mainly due to the relatively small optical scan angle. The TOSA can be increased

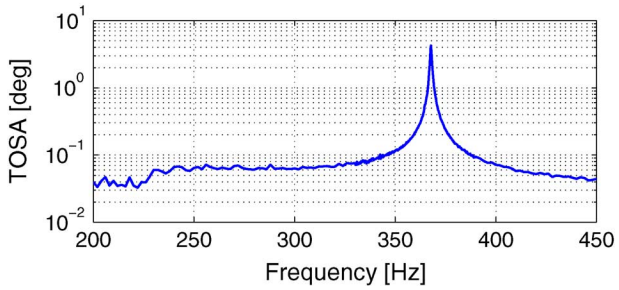

Fig. 4. Dynamic behavior of the device. (a) Slow-scan resonance characteristics of the electromagnetic actuator obtained at low drive levels. (b) Scanline created by the device at 20 cm away from the mirror when driven with 60-Hz sinusoidal current. (c) Fast-scan performance obtained using low power drive ($Q = 2700$).

TABLE I
COMPARISON OF SCANNERS WITH $Ni_{80}Fe_{20}$ OF VARIOUS THICKNESSES

Sample	Sample-I	Sample-II	Sample-III
Average thickness (t) [μm]	29	54	300
Resonance frequency (f_0) [Hz]	300.16	320.54	267.1
Total optical scan angle [deg]	10	11	8
Q-factor	94	105	81.9
Power consumption [mW]	42.84	42.84	47.73
TOSA/Q [deg]	0.1064	0.1048	0.0977
TOSA/Q/t [(deg·μm)$^{-1}$]	0.0037	0.0019	0.0003

either 1) by fabricating a softer springs and lower mirror mass at the same time for not effecting the resonance frequency, or 2) by applying more torque to the device at the fast-scan resonance. The latter approach deals with design of a high-frequency electrocoil where bandwidth of the magnetic core has to be increased to reduce losses. It is worth remembering that the high Q-factor of each mode separates the slow- and fast-scan motions by suppressing all the other spurious drive components due to the strong built-in mechanical bandpass filters.

An important observation can be drawn by examining the same mechanical design with different magnetic material thicknesses. Equation (1) assumes a high shape anisotropy and yields in forces that are directly proportional to the volume of the magnetic material. Nevertheless, one cannot increase the thickness of the magnetic layer indefinitely to get more magnetic force, since the shape anisotropy assumption would be violated after a certain thickness. This is experimentally verified and the results are summarized in Table I. Samples I and II has about the same TOSA normalized with Q-factor, while the NiFe thickness is nearly double in Sample II. Sample III has less TOSA$/Q/t$ with thicker NiFe layer and when normalized with NiFe thickness (TOSA$/Q/t$), Sample I gives the best performance. Therefore, for a given scanner geometry, there is a critical thickness where the performance peaks to the maximum.

IV. CONCLUSION AND DISCUSSION

A novel microscanner actuation mechanism is presented to satisfy the performance requirements of the raster scanning mirrors. Atmospheric operation is enabled eliminating the expensive vacuum-sealed packaging needs, which in turn improves system performance yielding cheaper products. Resonant operation of the scanner allows filtering out the nonlinearities and hysteresis in the excitation torque, which is inherent in this type of magnetic actuator. Fabricated using a bulk micromachining process, the present device is immune to the dynamic deformation and surface quality problems. Performance of the slow axis ($\theta \cdot D = 132^{\circ} \cdot$ mm) is sufficient to resolve 2000 pixels. However, if operated in 2-D mode as a display system at 60-Hz refresh rate, one can construct a 50×600 pixel display module with this scanner [3]. A number of light sources can be tiled to form a 2-D display with more desired aspect ratios such as 4 : 3 [12]. In order to prevent problems related to the flux leakage, the device is intended to be packaged in a Covar shield, where the scanner will also be fixed with a certain noncritical offset to the flux generator. There are a number of applications where the present device can directly be used. These include 1-D and 2-D barcode reading applications, resonant mode display, and imaging applications.

ACKNOWLEDGMENT

The authors would like to thank Microvision Corporation for the samples.

REFERENCES

[1] A. D. Yalcinkaya, H. Urey, T. Montague, D. Brown, and R. Sprague, "Two-axis electromagnetic microscanner for high reslolution displays," *IEEE J. Microelectromech. Syst.*, vol. 15, no. 4, pp. 786–794, Aug. 2006.

[2] R. Sprague, "MEMS device having simplified drive," U.S. Patent Appl. 20050253055, Nov. 17, 2005.

[3] H. Urey, "Retinal scanning displays," in *Encyclopedia of Optical Engineering*. New York: Marcel Dekker, Sep. 2003.

[4] G. Reyne, "Electromagnetic actuation for MOEMS, examples, advantages and drawbacks of MAGMAS," *J. Magn. Magn. Mat.*, vol. 242–245, pp. 1119–1125, 2002.

[5] A. D. Yalcinkaya, O. Ergeneman, and H. Urey, "Polymer magnetic scanner for bardcode reader applications," *Sens. Actuators A*, to be published.

[6] K. M.-H. Kiang, O. Solgaard, R. S. Muller, and K. Y. Lau, "Micromachined polysilicon microscanners for barcode readers," *IEEE Photon. Technol. Lett.*, vol. 8, no. 12, pp. 707–1709, Dec. 1996.

[7] C. Changho, K. Isamoto, and H. Toshiyoshi, "Optically modulated MEMS scanning endoscope," *IEEE Photon. Technol. Lett.*, vol. 18, no. 1, pp. 133–135, Jan. 1, 2006.

[8] J.-C. Tsai and M. C. Wu, "A high port-count wavelength-selective switch using a large scan-angle, high fill-factor, two axis MEMS scanner array," *IEEE Photon. Technol. Lett.*, vol. 18, no. 13, pp. 1439–1441, Jul. 1, 2006.

[9] G.-D. J. Su, L. Shi-Sheng, and M. C. H. Wu, "Optical scanners realized by surface-micromachined vertical torsion mirror," *IEEE Photon. Technol. Lett.*, vol. 11, no. 5, pp. 587–589, May 1999.

[10] K. Jongbaeg, D. Christensen, and L. Lin, "Monolithic 2-D scanning mirror using self-aligned angular vertical comb drives," *IEEE Photon. Technol. Lett.*, vol. 17, no. 11, pp. 2307–2309, Nov. 2005.

[11] H. Miyajima, N. Asaoka, M. Arima, Y. Minamoto, K. Murakami, and K. Matsumoto, "A durable, shock-resistant electromagnetic optical scanner with polyimide-based hinges," *IEEE J. Microelectromech. Syst.*, vol. 10, no. 3, pp. 418–424, Sep. 2001.

[12] H. Urey, "Scanned display with switched feeds and distortion correction," U.S. Patent 6 795 221, 2004.

[13] C. Liu and Y. W. Yi, "Micromachined magnetic actuators using electroplated permalloy," *IEEE Trans. Magn.*, vol. 35, no. 3, pt. 2, pp. 1976–1985, May 1999.

[14] H. Urey, A. D. Yalcinkaya, S. O. Isikman, O. Ergeneman, and S. Holmstrom, "Electromagnetic actuators for scanners," in *Proc. 20th Eur. Conf. Solid-State Tranducers*, Goteborg, Sweden, 2006, pp. 290–291.